Effect of Mesoscale Crystalline Structure on the Field-Effect Mobility of Regioregular Poly(3-hexyl thiophene) in Thin-Film Transistors

ARTICLE *in* ADVANCED FUNCTIONAL MATERIALS · APRIL 2005

Impact Factor: 11.81 · DOI: 10.1002/adfm.200400297

6 AUTHORS, INCLUDING:

Haiqin Yang
The Chinese University of Hong Kong
297 PUBLICATIONS **4,443** CITATIONS
SEE PROFILE

Tae Joo Shin
Ulsan National Institute of Science and Tec…
127 PUBLICATIONS **2,604** CITATIONS
SEE PROFILE

Chang Y. Ryu
Rensselaer Polytechnic Institute
81 PUBLICATIONS **2,209** CITATIONS
SEE PROFILE

ADVANCED FUNCTIONAL MATERIALS

Effect of Mesoscale Crystalline Structure on the Field-Effect Mobility of Regioregular Poly(3-hexyl thiophene) in Thin-Film Transistors

By *Hoichang Yang*, *Tae Joo Shin*, *Lin Yang*, *Kilwon Cho*, *Chang Y. Ryu*,* and *Zhenan Bao**

Regioregular poly(3-hexyl thiophene) (RR P3HT) is drop-cast to fabricate field-effect transistor (FET) devices from different solvents with different boiling points and solubilities for RR P3HT, such as methylene chloride, toluene, tetrahydrofuran, and chloroform. A Petri dish is used to cover the solution, and it takes less than 30 min for the solvents to evaporate at room temperature. The mesoscale crystalline morphology of RR P3HT thin films can be manipulated from well-dispersed nanofibrils to well-developed spherulites by changing solution processing conditions. The morphological correlation with the charge-carrier mobility in RR P3HT thin-film transistor (TFT) devices is investigated. The TFT devices show charge-carrier mobilities in the range of $10^{-4} \sim 10^{-2}$ $cm^2 V^{-1} s^{-1}$ depending on the solvent used, although grazing-incidence X-ray diffraction (GIXD) reveals that all films develop the same π–π-stacking orientation, where the <100>-axis is normal to the polymer films. By combining results from atomic force microscopy (AFM) and GIXD, it is found that the morphological connectivity of crystalline nanofibrils and the <100>-axis orientation distribution of the π–π-stacking plane with respect to the film normal play important roles on the charge-carrier mobility of RR P3HT for TFT applications.

1. Introduction

There has been great interest recently in the development of electrical devices and displays using solution-processable fabrication methods such as screen printing and ink-jet printing.[1–11] This trend is driven by the demands for inexpensive, flexible, and light-weight devices. Regioregular poly(3-hexyl thiophene) (RR P3HT) shows high field-effect mobility ($0.01 \sim 0.1$ $cm^2 V^{-1} s^{-1}$) and reasonable on/off ratios (> 100 in air and 10^6 in an inert atmosphere).[12,13] It has a regular end-to-end arrangement of side chains allowing efficient π–π-stacking of the conjugated backbones.[14] Its high solubility in various organic solvents and good film-forming properties also make it attractive as a printable semiconducting polymer.[15] The crystalline portion can transfer electrons through intra-chain and inter-chain transport, whereas the amorphous portion does the same through hopping or tunneling processes.[16] It has been shown that high regioregularity is required for the formation of highly ordered thin films, resulting in high charge-carrier mobility.[12] Sirringhaus et al. first reported that molecular weight (M_w, weight-average molecular weight) has considerable impact on the crystalline connectivity and ordering of P3HT spin-cast films.[17] Recently, Kline et al. observed that the mobility values differ by at least four orders of magnitude depending on the M_w of the polymer.[18]

The crystallinity and the crystalline-domain orientation of P3HT thin films depend not only on molecular properties, such as regioregularity, M_w, and molecular weight distribution, but also on processing conditions. Film deposition using solvents with different boiling points resulted in very different field-effect mobilities.[12,19] For the self-organized lamellar structure of P3HT with two-dimensional (2D) conjugated sheets, Sirringhaus et al. suggested that the π–π-stacking crystalline planes adopt two different orientations (parallel and normal to the substrate), depending on processing conditions and P3HT regioregularity.[17] Moreover, for regiorandom P3HT, Kobashi and Takeuchi found that the extent of main-chain stacking with the side chains acting as spacers was homogeneous in the spin-cast film, whereas it was inhomogeneous in the solvent-cast film containing well-developed face-to-face inter-chain stacking.[20] Liu et al. suggested that the strong tendency of RR P3HT to self-assemble into stacked aggregates is suppressed by fast solvent evaporation rates.[21]

In this paper, we report detailed morphological studies of drop-cast RR P3HT thin films using atomic force microscopy (AFM) and grazing-incidence X-ray diffraction (GIXD), and investigate the correlations between morphology and charge-carrier mobility for organic field-effect transistor (OFET) applications. Four different solvents—toluene, methylene chloride (CH_2Cl_2), chloroform ($CHCl_3$), and tetrahydrofuran

[*] Prof. C. Y. Ryu, Dr. H. Yang
Rensselaer Nanotechnology Center, Rensselaer Polytechnic Institute
Troy, NY 12180 (USA)
E-mail: ryuc@rpi.edu
Prof. Z. Bao
Department of Chemical Engineering
Stanford University
Stanford, CA 94305 (USA)
E-mail: zbao@chemeng.stanford.edu
Dr. T. J. Shin, Dr. L. Yang
BNL, National Synchrotron Light Source
Upton, NY 11973 (USA)
Dr. H. Yang, Prof. K. Cho
Department of Chemical Engineering
Pohang University of Science and Technology
Pohang, 790-784 (Korea)

 DOI: 10.1002/adfm.200400297

(THF)—were employed to manipulate the mesoscale crystalline morphology of drop-cast RR P3HT films ranging from well-dispersed nanometer-scale fibrils to well-developed spherulites.

2. Results and Discussion

Thermal analysis of RR P3HT using a differential scanning calorimeter (DSC) supports the notion that it is a semicrystalline polymer with a melting peak at ~216 °C and a crystallization peak at 179 °C on heating and cooling, respectively (Fig. 1). The relatively low crystallinity of RR P3HT, which is about 15 %, as determined from heat of melting,[22] could be attributed to the soft impingement of alkyl side chains by the

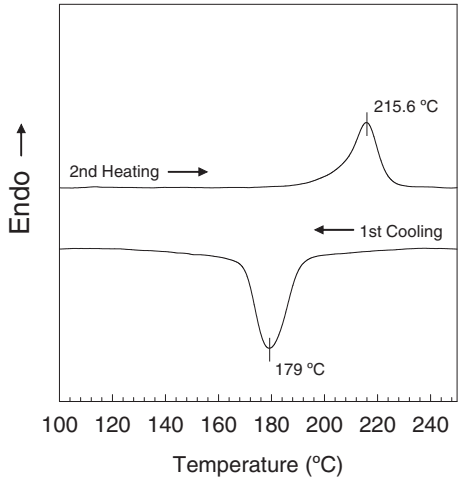

Figure 1. DSC curves of as-received RR P3HT. (Heating and cooling rates were 10 °C min^{-1}.)

rigid amorphous portions hindering the crystalline-domain formation from RR P3HT chains.[23,24] In molten or solution state, the polymer main chain may adopt a coiled conformation; in order to crystallize into the crystalline lattice, it has to be straightened. However, the side chains may not favor the unfolding process readily, resulting in low crystallinity. The Huggins constant of RR P3HT is 0.58 in THF, corresponding to a typical value for flexible polymers.[25] Specifically, interactions between the solvent and P3HT polymer can change the crystallinity and morphology of P3HT thin films during solvent evaporation upon drop-casting. The semicrystalline RR P3HT films consist of relatively ordered (crystalline) regions and disordered (amorphous) regions, and Masubuchi and Kazama reported that the amorphous regions have lower charge-carrier mobility than the crystalline domains.[16] In addition, a large increase in resistance at the grain boundaries between polycrystalline domains of conducting organic materials has also been observed.[26] Therefore, crystalline-domain "connectivity" is one of the key determining factors for thin-film transistor (TFT) charge-carrier mobility.

The field-effect mobilities of RR P3HT were measured using the bottom-contact thin-film field-effect transistor (FET) geometry, similar to that reported previously (Fig. 2a, inset).[27] The P3HT films were drop-cast onto a SiO_2 dielectric layer from solutions of the polymer (0.25 wt.-%) in different solvents (CH_2Cl_2, toluene, $CHCl_3$, and THF).[28] A Petri dish was

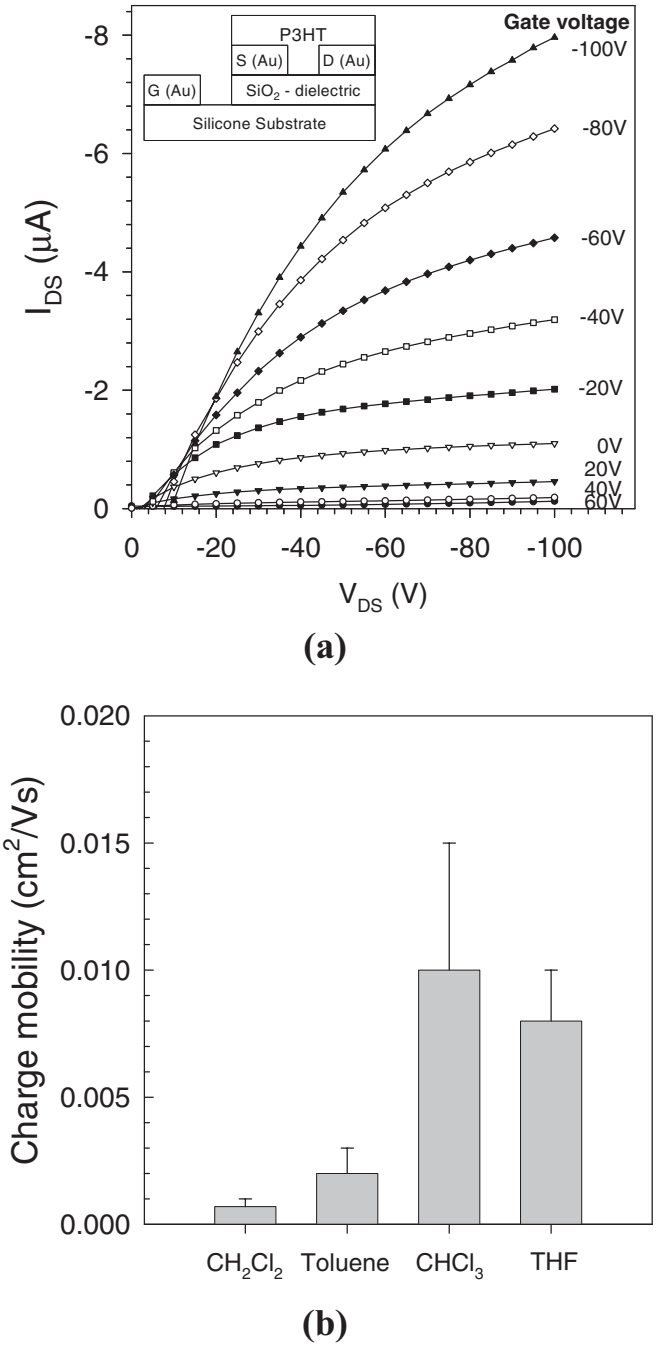

Figure 2. a) *I–V* characteristics of FET device containing RR P3HT film made from $CHCl_3$ solution (I_{DS}: drain–source current; V_{DS}: drain–source voltage). The inset shows a schematic diagram of the device structure: S: source; D: drain; G: gate. b) Plot of field-effect mobility of RR P3HT versus the solvents used to drop-cast the films.

ADVANCED FUNCTIONAL MATERIALS

used to cover the solution and it took less than 30 min for the solvents to evaporate at room temperature. Figure 2a shows typical current–voltage (I–V) curves for a FET device containing P3HT film cast from $CHCl_3$ solution, operating in the accumulation mode. In the saturation region, the drain–source current (I_{DS}) can be described using the following equation,

$$I_{DS} = \frac{WC_i}{2L}\mu(V_G - V_0)^2 \quad (1)$$

where μ is the field-effect mobility, W (250 μm) is the channel width, L (12 μm) is the channel length, C_i is the capacitance per unit area of the insulating layer (SiO_2, 3000 Å, $C_i = 10$ nF cm^{-2}), and V_G and V_0 are the gate voltage and the extrapolated threshold voltage, respectively.

As seen in Figure 2b, the FET devices operating in the accumulation mode showed field-effect mobilities of the order of $10^{-4} \sim 10^{-2}$ cm^2 V^{-1} s^{-1}, depending on the solvents used for film deposition. We found that RR P3HT films drop-cast from $CHCl_3$ and CH_2Cl_2 displayed the highest (~ 0.01 cm^2 V^{-1} s^{-1}) and lowest ($\sim 10^{-4}$ cm^2 V^{-1} s^{-1}) field-effect mobilities, respectively. A solvent with a slower evaporation rate generally facilitates the growth of a highly crystalline film (confirmed by GIXD), and thus should be favorable for improving charge carrier mobility. However, the film cast from toluene, which is the solvent with the highest boiling point used in this study, showed low mobility of only $\sim 2 \times 10^{-3}$ cm^2 V^{-1} s^{-1}. Therefore, it is also important to examine details of the crystalline morphology of RR P3HT thin films prepared from different solvents to explain the measured differences in field-effect mobilities. Because thin-film crystallization is generally an exothermic process when the polymer reaches its solubility limit, the difference in heat capacity and the solubility parameter of solvents for RR P3HT should also be considered in addition to the solvent boiling points.

In order to measure the crystallinity and the crystalline ordering of RR P3HT in thin films, GIXD experiments were performed on drop-cast RR P3HT films. Figure 3 shows 2D GIXD patterns of RR P3HT films drop-cast on a SiO_2/Si substrate. All films have similar thicknesses of about 100 nm. To increase GIXD peak intensity for investigating the crystallinity and orientation that prevail throughout the film, we employed an incident angle ($\alpha = 0.3°$) slightly above the critical angle ($\alpha_c = 0.18°$).[17] For all drop-cast films, we observed the (100) peaks with higher-order peaks along the q_z-axis indicating that the <100>-axis of π–π-stacked crystalline planes of RR P3HT is preferentially oriented normal to the film. All four RR P3HT films drop-cast from different solvents showed the same preferential orientations determined by 2D GIXD, nevertheless, these films showed significantly different field-effect mobilities.

The effect of film casting solvent on the overall crystallinity and the crystalline-orientation distribution with respect to the substrate surface is also examined by GIXD. After correction for the film thickness, we found that the out-of-plane (100) peak intensities (Fig. 4a) follow the following order: THF ~ $CHCl_3$ > toluene > CH_2Cl_2. As Kline et al.[18] and Sirringhaus and co-workers[19] have suggested, the observed (100) in-

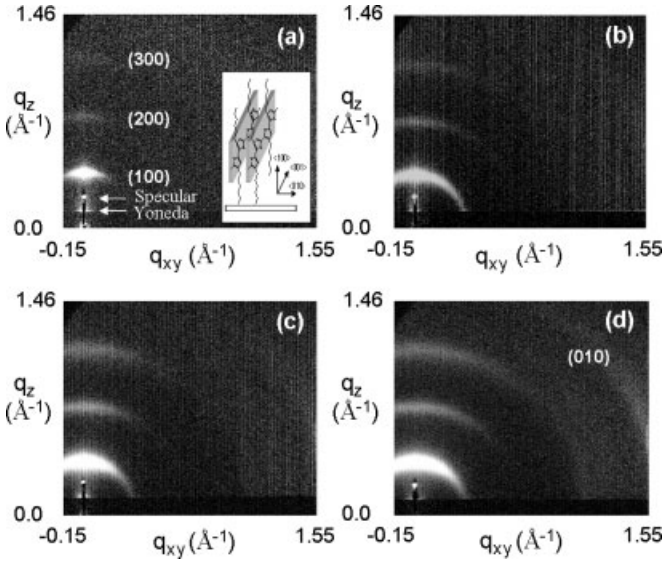

Figure 3. 2D GIXD patterns for P3HT thin films drop-cast from different solvents: a) CH_2Cl_2; b) toluene; c) $CHCl_3$; and d) THF. (The arrow-marked peaks are not from the polymer film.)

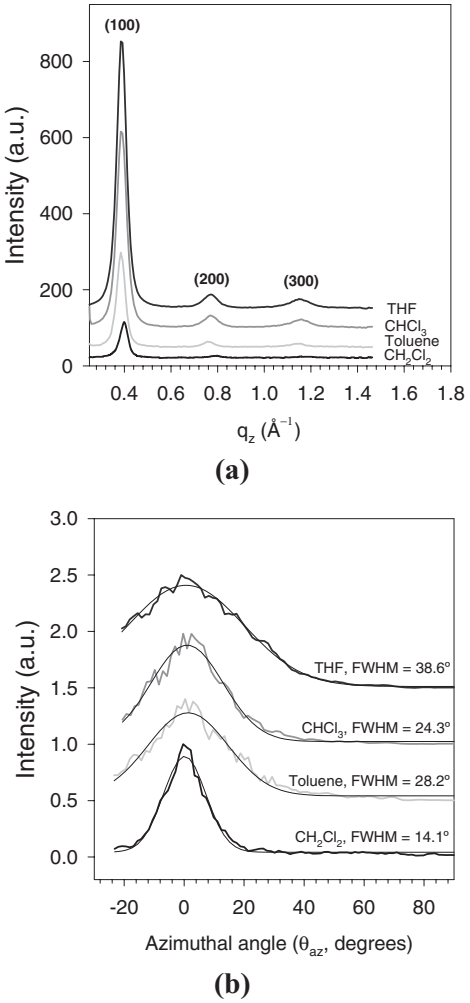

Figure 4. a) Out-of-plane X-ray diffraction (XRD) profiles of P3HT thin films; b) azimuthal XRD profiles of the films at q_z = (100) peak.

tensity from different solvents represents the degree of the overall crystallinity. In particular, Sirringhaus and co-workers recently reported that the solution "drying time" significantly affects the microcrystalline development, which correlates with charge mobility of RR P3HT in TFTs.[19] For the films prepared for our transistor studies, a Petri dish was used to cover the solution during solvent casting. We observed that $CHCl_3$ evaporates in 20 min, whereas CH_2Cl_2 evaporates in just 5 min. When we used a closed jar with a rubber stopper for solvent casting, it took about 2 h to remove both $CHCl_3$ and CH_2Cl_2 and we observed that the (100) out-of-plane GIXD intensities were similar for both P3HT films, suggesting that similar crystallinities developed during the solvent casting from $CHCl_3$ and CH_2Cl_2 solutions with similar solvent-evaporation rates in a closed jar.[29]

The full width half maximum (FWHM) of the azimuthal-angle intensity of the $q_z = (100)$ peaks (Fig. 4b) is also used to compare the broadness of the crystalline-plane orientation correlation with respect to the substrate surface. It was found that the FWHM of the film follows the order $CH_2Cl_2 < CHCl_3 <$ toluene $\ll$ THF. This suggests that the film drop-cast from THF has the broadest orientation distribution of the crystalline domains with respect to the substrate surface, even though it exhibits the highest crystallinity, similar to the film cast from $CHCl_3$. Note that the field-effect mobility is of the order $CHCl_3 >$ THF $\gg$ toluene $> CH_2Cl_2$ (Fig. 2b). The film drop-cast from THF solution did not show the highest mobility, despite of its crystallinity being highest, most likely because of the broad orientation distribution of crystalline domains with respect to the surface. The poor "alignment" of the <100>-axis of the conjugated plane on the substrate definitely interferes significantly with hopping of charge carriers through π–π-stackings between polymer chains. Therefore, our GIXD results suggest that both the orientation distribution and crystallinity of the crystalline domains affect the field-effect mobility of RR P3HT films and that there is an optimum solvent to prepare uniformly oriented and well-developed crystalline P3HT lamellae in order to achieve high field-effect mobilities in RR P3HT thin films.

The crystalline mesoscale morphology in the films' lateral direction was investigated using AFM. Polymer crystallization into a thin film from solution is a complex exothermic process, which could be affected by the solution properties, such as solubility, evaporation rate, heat capacity, and heat-transfer coefficient, in addition to the film thickness. Figure 5 shows AFM phase images of RR P3HT films solvent-cast onto a SiO_2 substrate, and the insets represent large-scale (10 μm × 10 μm) images of the crystalline morphologies of thin films prepared from different solvents. All the RR P3HT films form similarly nanometer-scale fibrillar crystalline domains (nanofibril domains), but the shape and connectivity of the nanofibril domains are very much dependent on the solvent used for drop-casting. The film made from toluene showed well-developed spherulites with lengths of 5 ~ 7 μm, which represents a typical superstructure of semicrystalline polymer lamellae. While a weak signature of spherulites could be observed in the $CHCl_3$-cast film, we could not find clear spherulitic signatures for CH_2Cl_2- and THF- cast films.

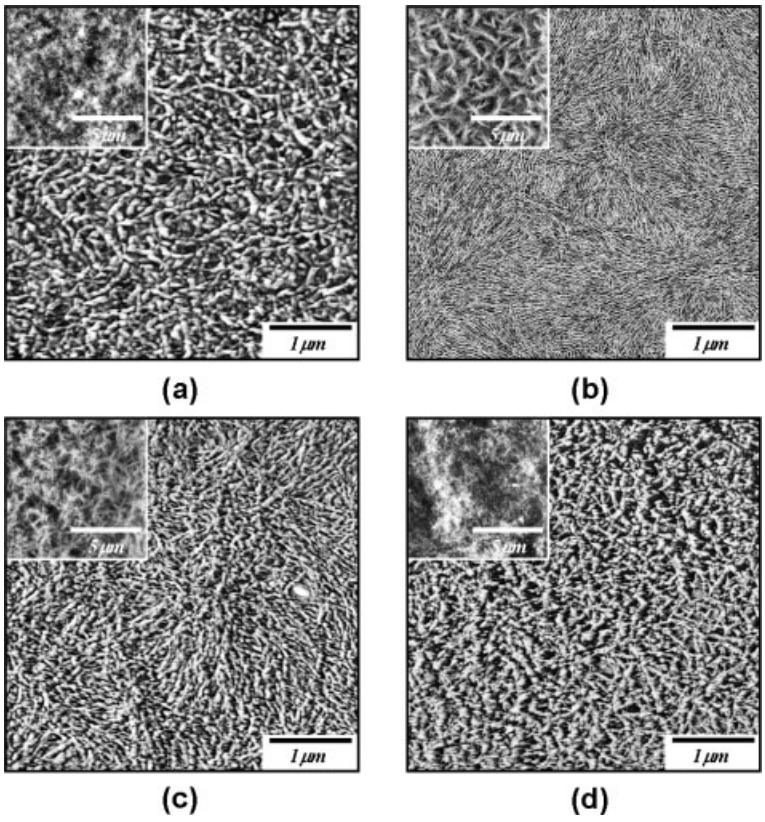

Figure 5. AFM images of P3HT films drop-cast on SiO_2 substrate from different solvents: a) CH_2Cl_2; b) toluene; c) $CHCl_3$; and d) THF. The insets represent AFM topography images with a larger scale.

For the same vertical orientation of stacked conjugated planes on the substrate surface (Fig. 3), the field-effect mobility is of the order $CHCl_3 >$ THF $\gg$ toluene $> CH_2Cl_2$ (Fig. 2b). It is expected that grain boundary and morphological connectivity of the crystalline nanofibrils will play important roles in affecting the field-effect mobility. For toluene-cast films, the overall crystalline structure in the film seems to be spherulitic with distinct grain boundaries, and the thickness of crystalline fibrils composing the spherulites is ~ 15 nm. This result is partly due to the slow evaporation rate of toluene (boiling point = 110.6 °C), which permits RR P3HT to grow into well-developed spherulites. On the other hand, the CH_2Cl_2-cast film showed a "matchstick-like" morphology, where short (~ 0.5 μm long) nanorod-like crystal domains were dispersed without connecting with each other. The weakly developed spherulites in the $CHCl_3$-cast film are composed of crystalline grains and nanofibrils whose spherulitic and fibrillar boundaries are not distinctly defined. The $CHCl_3$-cast film shows crystalline fibrils that are ~ 32 nm thick, branched, and eventually connected to other long nanofibrils (see Fig. 6b). The THF-cast films

ADVANCED FUNCTIONAL MATERIALS

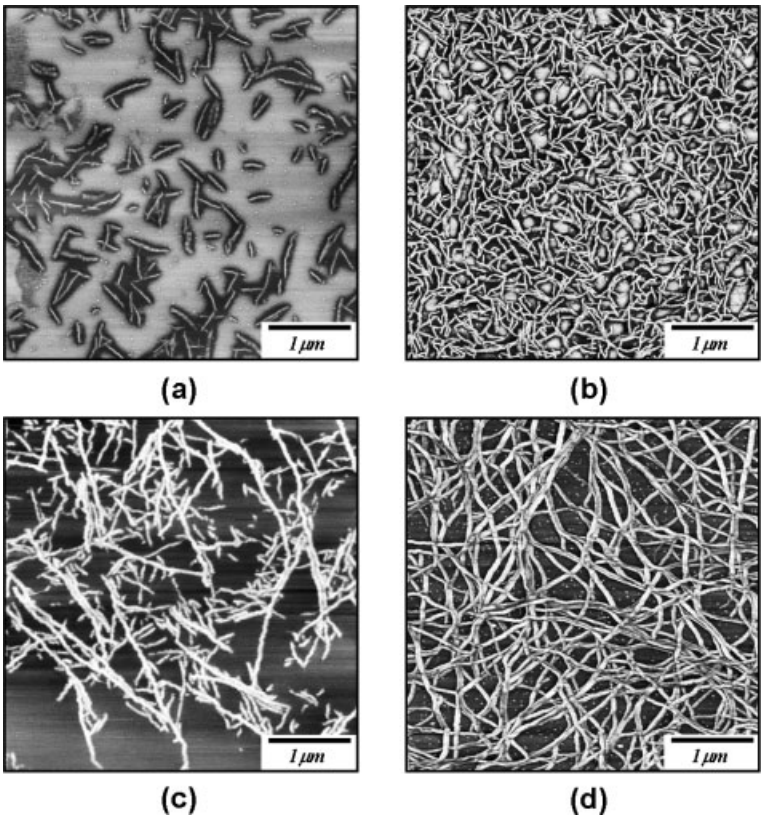

Figure 6. AFM phase images of RR P3HT films on SiO_2 substrates from 0.05 and 0.1 wt.-% solutions with different solvents: a) 0.05 and b) 0.1 wt.-% in CH_2Cl_2; c) 0.05 and d) 0.1 wt.-% in $CHCl_3$.

showed well-dispersed nanofibrils with irregular nodules forming an interconnected network of nanocrystalline fibrils as in the $CHCl_3$ sample. In the THF-cast film, we attribute the broadening of the <100>-orientation from GIXD to the irregular nodule morphology observed by AFM, since the irregular nodules should disturb the uniform vertical stacking of the conjugated planes with respect to the substrate surface.

It has been previously shown that grain boundaries limit the field-effect mobility in organic transistors made using oligothiophenes, and RR P3HT with low molecular weights (3.2 kg mol^{-1}).[17,30] Recently, Kelley and Frisbie reported that the grain-boundary effect on conductivity of sexithiophene crystals using a conducting atomic-force microscope (C-AFM).[31] They found that the resistance across the grain boundary increased significantly and suggested that grain boundaries result in a high-energy barrier for charge transfer. Recently, others have suggested that charge carriers and excitons in RR P3HT delocalize over several neighboring chains locally aligned by π-stacking.[32,33] This delocalization over several chains makes it easier for the charge carriers to bypass single chain defects that would stop the carrier on an isolated chain, whereas grain boundaries would disrupt charge transport.

In order to investigate the interconnected morphology of the nanofibrillar crystalline domains, we diluted the CH_2Cl_2 and $CHCl_3$ solutions for drop-casting. As shown in Figure 6a, the film cast from 0.05 wt.-% CH_2Cl_2 solution revealed individual crystalline domains of discrete short (~500 nm) nanorod-like shapes. When the concentration was increased to 0.1 wt.-%, the surface coverage of the short nanorod-like crystallites increased while retaining their good dispersion, and uniformly-coated RR P3HT films were formed. When the film was prepared from $CHCl_3$ solution (Fig. 6b), the length of the nanofibrils significantly increased with pronounced branching, resembling the fractal growth observed during the diffusion-limited 2D crystallization of poly(ethylene oxide).[34–36] We observed that the branched nanofibrils grow from several-micrometer-long primary nanofibrillar crystals (in the films cast from the 0.05 wt.-% $CHCl_3$ solution), and then all the branched longer nanofibrillar crystalline domains eventually form a networked morphology at a higher concentration of 0.1 wt.-% in $CHCl_3$. Although both CH_2Cl_2- and $CHCl_3$-cast films posses good interconnectivities of nanorod-like crystalline domains from solvent casting at 0.1 wt.-%, the interconnected morphology should be significantly different. Because the microscrytalline domains from CH_2Cl_2 casting display short rod-like domains without crystalline branching, their interconnection must occur mainly via physical contacts. In contrast, the long rod-like microcrystallites with multiple branching cast from the $CHCl_3$ solution are highly likely to form interconnection via crystalline branching. In addition, the $CHCl_3$-cast films form nanofibrillar networks without developing distinct grain boundaries (Fig. 5c). We attribute the high charge mobility in the $CHCl_3$-cast film to the highly interconnected nanofibrillar networks formed via crystalline branching that serve as charge-transport conduits.

3. Conclusion

We have investigated correlations between the crystalline morphology and field-effect mobility of drop-cast RR P3HT films by inducing different crystalline morphologies using different solvents. A Petri dish was used to cover the solution, where solvents were evaporated in less than 30 min. We found that all the drop-cast films develop the π–π lamellar stacking perpendicular to the substrate surface and that the field-effect mobility was of the order $CHCl_3 > THF \gg$ toluene $> CH_2Cl_2$. There are two major morphological factors that affect the field-effect mobility for the same perpendicular lamellar orientation: 1) The azimuthal angle FWHM of the (100) peak, which measures broadness of the <100> orientation correlation with respect to the substrate surface was in the order $CH_2Cl_2 < CHCl_3 <$ toluene $\ll$ THF and 2) mesoscale morphological features, such as development of a distinct grain boundary, and the length and branching of nanofibrillar crystalline domains and their interconnectivity. The significantly low charge mobility in toluene and CH_2Cl_2-cast films can be attributed to the distinct spherulitic grain boundary and the short

nanorod-like fibrils ("matchstick-like" morphology) via physical contacts, respectively. The $CHCl_3$-cast film, which shows the highest field-effect mobility, forms highly interconnected nanofibrillar networks via microdomain branching that serve as charge transport conduits without developing distinct grain boundaries. The significant broadening of the (100)-plane orientation distribution in the THF-cast film from GIXD correlated with the irregular nodule morphology from AFM, where the uniform vertical organization of the conjugated planes is disturbed and the charge transport is hampered more than in the case of the $CHCl_3$-cast film.

4. Experimental

RR P3HT (number-average molecular weight, $M_n = 11\,400$ g mol^{-1}; polydispersity index, PDI = 2.2) and high-performance liquid chromatography (HPLC)-grade solvents were purchased from Aldrich Chemical Co. and used as received. Thermal behavior of RR P3HT was measured using a differential scanning calorimeter (DSC, Perkin–Elmer DSC 7). Approximately 10 mg of sample was loaded into a solid-type pan, heated and cooled at a rate of 10 °C min^{-1} under N_2 gas. The schematic diagram of the transistor device structure is shown in the inset of Figure 2a and its preparation has been described previously: W (250 μm) is the channel width, L (12 μm) is the channel length, and C_i is the capacitance per unit area of the insulating layer (SiO_2, 3000 Å, $C_i = 10$ nF cm^{-2}). Thin films of RR P3HT were prepared by drop-casting from different solvents (CH_2Cl_2, toluene, $CHCl_3$, and THF) and the thickness of the films was about 100 nm when using a solution concentration of 0.25 wt.-%. All solutions were filtered through a 0.20 μm-pore-size poly(tetrafluoroethylene) (PTFE)-membrane syringe filter prior to usage and a Petri dish was used to cover the solution as it took less than 30 min for the solvents to evaporate at room temperature. The electrical characteristics of the FET devices were measured under accumulation mode using a Hewlett–Packard (HP) 4145B parameter analyzer. AFM experiments for drop-cast RR P3HT films were performed with a Multimode Nanoscope IIIa (Digital Instruments/Veeco Metrology Group) atomic force microscope. AFM topography and phase images were recorded simultaneously in tapping mode. The driving frequency was adjusted to the resonant frequency (~70 kHz) of the probe in the immediate vicinity of a sample surface. A higher value for the drive amplitude of probe oscillation (about twice than that of the initial approaching one) for imaging was chosen to maximize the image contrast, as drop-cast thin films have a wetting surface layer without features [21]. 2D GIXD experiments on drop-cast P3HT thin films were performed at the X21 beam line of Brookhaven National Light Source (BNLS). The sample was mounted on a two-axis goniometer and the scattered intensity was recorded by a 2D gas proportional detector (Ar/CO_2 (80:20) mixture). The 2D GIXD patterns were obtained in the range of $0 < q_z < 1.46$ Å^{-1} and $0 < q_{xy} < 1.55$ Å^{-1} (xy and z: parallel and normal to the substrate, respectively). The incident-beam angle was higher than 0.18° in order to remove the Si(100) peak.

Received: July 2, 2004
Final version: September 19, 2004

[1] A. J. Lovinger, L. J. Rothberg, *J. Mater. Res.* **1996**, *11*, 1581.
[2] H. E. Katz, *J. Mater. Chem.* **1997**, *7*, 369.
[3] F. Garnier, R. Hajlaoui, A. Yassar, P. Strivastava, *Science* **1994**, *265*, 1684.
[4] A. Tsumura, H. Koezuka, T. Ando, *Appl. Phys. Lett.* **1986**, *49*, 1210.
[5] H. Koezuka, A. Tsumura, T. Ando, *Synth. Met.* **1987**, *18*, 699.
[6] J. Paloheimo, P. Kuivalainen, H. Stubb, E. Vuorimaa, P. Y. Lahti, *Appl. Phys. Lett.* **1990**, *56*, 157.
[7] K. Yoshino, H. Takahashi, K. Muro, Y. Ohmori, R. Sugimoto, *J. Appl. Phys.* **1991**, *70*, 5035.
[8] Y. Ohmori, K. Muro, M. Uchida, T. Kawai, K. Yoshino, *Jpn. J. Appl. Phys.* **1991**, *30*, L610.
[9] A. Assadi, C. Svensson, M. Willander, O. Inganas, *Appl. Phys. Lett.* **1988**, *53*, 195.
[10] A. R. Brown, A. Pomp, C. M. Hart, D. M. de Leeuw, *Science* **1995**, *270*, 972.
[11] H. Fuchigami, A. Tsumura, H. Koezuka, *Appl. Phys. Lett.* **1993**, *63*, 1372.
[12] Z. Bao, A. Dodabalapur, A. J. Lovinger, *Appl. Phys. Lett.* **1996**, *69*, 4108.
[13] H. E. Katz, Z. Bao, *J. Phys. Chem. B* **2000**, *104*, 671.
[14] T. Yamamoto, D. Komarudin, M. Arai, B. Lee, H. Suganuma, N. Asakawa, Y. Inoue, K. Kubota, S. Sasaki, T. Fukuda, H. Matsuda, *J. Am. Chem. Soc.* **1998**, *120*, 2047.
[15] Z. Bao, Y. Feng, A. Dodabalapur, V. R. Raju, A. J. Lovinger, *Chem. Mater.* **1997**, *9*, 1299.
[16] S. Masubuchi, S. Kazama, *Synth. Met.* **1995**, *74*, 151.
[17] H. Sirringhaus, P. J. Brown, R. H. Friend, M. M. Nielsen, K. Bechgaard, B. M. W. Langeveld-Voss, A. J. H. Spiering, R. A. J. Janssen, E. W. Meijer, P. Herwig, D. M. de Leeuw, *Nature* **1999**, *401*, 685.
[18] R. J. Kline, E. N. Kadnikova, J. Liu, J. M. J. Frechet, M. D. McGehee, *Adv. Mater.* **2003**, *15*, 1519.
[19] J. Chang, B. Sun, D. W. Breiby, M. M. Nielsen, T. I. Sölling, M. Giles, I. McCulloch, H. Sirringhaus, *Chem. Mater.* **2004**, *16*, 4772.
[20] M. Kobashi, H. Takeuchi, *Macromolecules* **1998**, *31*, 7273.
[21] J. Liu, E. Sheina, T. Kowalewski, R. D. McCullough, *Angew. Chem. Int. Ed.* **2002**, *41*, 329.
[22] S. Malik, A. K. Nandi, *J. Polym. Sci., Part B: Polym. Phys.* **2002**, *40*, 2073.
[23] S. Z. D. Cheng, B. Wanderlich, *Macromolecules* **1988**, *21*, 3327.
[24] S. Z. D. Cheng, *Macromolecules* **1988**, *21*, 2475.
[25] G. W. Heffner, D. S. Pearson, *Macromolecules* **1991**, *24*, 6295.
[26] H. Meng, J. Zhang, A. J. Lovinger, B. Wang, P. G. V. Patten, Z. Bao, *Chem. Mater.* **2003**, *15*, 1778.
[27] S. M. Sze, in *Physics of Semiconductor Devices*, Wiley, New York **1981**.
[28] Methylene chloride (CH_2Cl_2, boiling point (bp): 40 °C, vapor pressure (vp): 350 mmHg (at 20 °C)); chloroform ($CHCl_3$, bp: 61 °C, vp: 159 mmHg (at 20 °C)); tetrahydrofuran (THF, bp: 65 °C, vp: 129 mmHg (at 20 °C)); toluene (bp: 110 °C, vp: 47 mmHg (at 20 °C))
[29] H. Yang, T. J. Shin, C. Y. Ryu, Z. Bao, manuscript in preparation.
[30] G. Horowitz, *Adv. Mater.* **1998**, *10*, 365.
[31] T. W. Kelley, C. D. Frisbie, *J. Phys. Chem. B* **2001**, *105*, 4538.
[32] D. Beljonne, J. Cornil, H. Sirringhaus, P. J. Brown, M. Shkunov, R. H. Friend, J. L. Bredas, *Adv. Funct. Mater.* **2001**, *11*, 229.
[33] X. M. Jiang, R. Österbacka, O. Korovyanko, C. P. An, B. Horovitz, R. A. J. Janssen, Z. V. Vardeny, *Adv. Funct. Mater.* **2002**, *12*, 587.
[34] M. T. Wang, H. G. Braun, E. Meyer, *Macromolecules* **2004**, *37*, 437.
[35] G. Reither, J. U. Sommer, *J. Chem. Phys.* **2000**, *112*, 4376.
[36] J. U. Sommer, G. Reither, *J. Chem. Phys.* **2000**, *112*, 4384.

